









Stratospheric ozone depletion in the Antarctic region triggers intense changes in sea salt aerosol geochemistry

Sérgio J. Gonçalves Jr ^{1,2}, Heitor Evangelista², Johannes Weis ^{3,4,5}, Tristan H. Harder^{3,4,5}, Swarup China⁶, Simon Müller^{3,4}, Magdalena M. Marques⁷, Newton de Magalhães Neto^{2,8}, Heber R. Passos⁹, Marcelo Sampaio ⁹, Jefferson C. Simões ^{7,10}, Bruno Vinícius Ximenes de Oliveira ², Carlos I. Yamamoto¹¹, Alexander Laskin ^{6,12}, Mary K. Gilles ³ & Ricardo H. M. Godoi¹

Since the early 1980s, the Antarctic environment has served as a natural field laboratory for researchers to investigate the effects of stratospheric ozone depletion, which has resulted in increased surface ultraviolet radiation levels. However, its effective threats still present gaps. We report new pieces of evidence of increased ultraviolet radiation impacting West Antarctica sea salt aerosols. Salt aerosols, particularly in the Southern Ocean Sea, play an important role in the radiative earth balance. To disclose the molecular details of sea salt aerosols, we used a synchrotron-based multi-element microscopic speciation of individual microparticles (Scanning Transmission X-ray Microscopy with Near-Edge X-ray Absorption Fine Structure Spectroscopy combined with Computer-Controlled Scanning Electron Microscopy). Here we identified substantial abundances of chlorine-enriched aerosols in sea salt generated by photolytic products, whereas ice core records revealed increased chlorine depletion from the onset of ozone depletion. Our findings reveal that modern sea salt modification has no Holocene precedent.

¹Environmental Engineering Department, Federal University of Paraná (UFPR), Curitiba, Brazil. ²LARAMG, Rio de Janeiro State University (UERJ), Rio de Janeiro, Brazil. ³Chemical Sciences Division, Lawrence Berkeley National Laboratory, Berkeley, CA, USA. ⁴Department of Chemistry, University of California, Berkeley, CA, USA. ⁵Physikalisches Institut, Universität Würzburg, Würzburg, Germany. ⁶William R. Wiley Environmental and Molecular Sciences Laboratory, Pacific Northwest National Laboratory, Richland, WA, USA. ⁷Polar and Climatic Center, Institute of Geosciences, Federal University of Rio Grande do Sul (UFRGS), Porto Alegre, Brazil. ⁸LAGEPRO, Rio de Janeiro State University (UERJ), Rio de Janeiro, Brazil. ⁹Brazilian National Space Institute (INPE), São José dos Campos, Brazil. ¹⁰Climate Change Institute, University of Maine, Orono, ME, USA. ¹¹Chemical Engineering Department, Federal University of Paraná (UFPR), Curitiba, Brazil. ¹²Department of Chemistry, Purdue University, West Lafayette, IN, USA. ✉email: sjrgoncalves@gmail.com

The unprecedented man-induced depletion of stratospheric ozone was first reported in 1985, but the depletion is evident in observations of total ozone from the mid-70's over the Antarctic region¹. By now, almost fifty years later, several works have evidenced its impacts from the atmospheric chemistry and circulation^{1,2}, to the terrestrial and marine polar ecosystems^{3–6}, as a consequence, increased incidence of UV-B (ultraviolet radiation at 280–320 nm) at the surface. During the pre-ozone depletion period, UV-B levels in Antarctica varied seasonally, with maximum values around the summer solstice in December. Since the onset of stratospheric ozone depletion, the maximum has shifted to the spring season. Despite this change in time and intensity, previous work showed that actual UV-B levels in the summer season increased by approximately 15% when compared with the same period before the ozone depletion^{7,8}. Since the Antarctic troposphere is now exposed to dramatically higher quantities of UV-B radiation, it is no longer in a “natural” state^{8,9}. Among the impacts on the atmospheric chemistry by ozone hole and UV-B incidence, the investigation of sea salt aerosols plays a critical role, as it takes part in radiative processes at the maritime boundary layer^{10,11}.

In polar regions, sea salt aerosols emissions are caused mainly by: the release from the ocean's surface reaching the boundary layer from mechanical wave processes of bursting air bubbles during wave breaking at surface oceans by winds¹²; from frost flowers, at the newly-formed sea-ice surface during the winter, and blowing snow above sea ice^{13–15}. Their interaction with inorganic acids in the atmosphere, such as nitric acid (HNO₃) and sulfuric acid (H₂SO₄), and gases like nitrogen dioxide (NO₂) and sulfur dioxide (SO₂), through heterogeneous reactions, releases hydrochloric acid (HCl) and others gaseous reactive chlorine compounds, such as chlorine gas (Cl₂), chlorine nitrite (ClNO₂), and hypochlorous acid (HOCl)^{16–18}. Consequently, a deficit of chloride ion (Cl⁻) relative to sodium ion (Na⁺) is observed in processed sea salt particles over the open ocean, the sea ice, and the continental ice when compared to fresh sea salt^{19–22}.

In the Antarctic Maritime environment, an 8-year aerosol continuous monitoring conducted at South Shetland Islands²³ demonstrated that atmospheric chlorine deficit is enhanced, especially in the fine mode particles and during the austral summer, when the regional primary productivity reaches a maximum. Although the deficit Cl⁻ is partially related to organic acids, such as oxalic acid, fulvic acid, and malonic acid²⁴, due to the deficiency of organic emissions in the Antarctic environment, the Cl⁻ depletion is predominantly associated with particle processing by inorganic acids¹⁷. However, not all sea salt particles interact with acids (e.g., the sulfatization process could occur) in the marine environment²⁵. A fraction of unreacted particles is transported inland over the Antarctic ice sheet. At Talos Dome/East Antarctica, it was estimated that, from the molar ratio of sodium chloride and sodium sulfate (NaCl/Na₂SO₄), around half of the sea salt has not undergone any sulfatization all along the late Holocene²⁵.

HCl and other gas-phase Cl-containing species released from atmospheric sources and reactions (including acid displacement in sea salt particles) are ‘sticky’ gas-phase species that get adsorbed on the surfaces of atmospheric ice (snowflakes), which eventually precipitates out and form snowpack. Sea salt particles deposited onto the ice sheet undergo secondary depletion processes: the snowpack acts as a potent source of trace reactive compounds (hydroxide (OH), ozone (O₃), and NO₂) that can interact with airborne sea salt in the overlying atmosphere. The photochemical processes^{9,26} constrain the emission of these gases, and an enhanced UV-B radiation flux due to the stratospheric ozone depletion in Antarctica plays a role in adding a “photochemical depletion factor”⁹. In the troposphere, chlorine

atoms react rapidly with O₃ forming chlorine monoxide (ClO)^{17,27,28}. The Cl⁻ has a low energy level when thermodynamically compared with other species ($\Delta_f G^\circ(\text{Cl}^-_{\text{(aq)}}) = -131 \text{ kJ mol}^{-1}$), but is very stable and favorable to react chemically, forming chlorine oxides species^{28,29}. Measurements performed from the marine coastal areas towards the inland in East Antarctica showed that the ratios of chloride related to sodium (Cl/Na) of surface snow samples change from that of bulk seawater value to a slight Cl⁻ depletion from a ratio value of 3.0³⁰ approximately.

To deepen our understanding of the multiple sea salt interactions in the Antarctic boundary layer, we have conducted a microscopic/molecular speciation of individual aerosol micro-particles collected in continental West Antarctica. We used a synchrotron-based multi-element Scanning Transmission X-ray Microscopy with near-edge X-ray absorption fine structure spectroscopy (STXM/NEXAFS)³¹ combined with Computer-Controlled Scanning Electron Microscopy coupled with an Energy Dispersive X-ray detector (CCSEM/EDX). In a complementary way, we investigated, from ice core ionic data, the overall impact of the enhanced UV-B radiation based on the Cl/Na ratios (mass ratios) before and during (since the 1960s) the ozone depletion periods in the Antarctic region, as well as in the Holocene time scale.

Results and discussions

During the aerosol samplings at Criosfera 1 lab (84°00'S; 79°30'W), the origin of sea salt was dominated by the advection of air masses coming from two distinct geographical influences: (1) between December 19th to 21st, 2014, when air masses migrated from the Weddell Sea sector to module Criosfera 1 lab (Fig. 1a), covering a distance of approximately 2000 km over sea ice and the ice sheet, with higher marine influence. In this case, sea salt aerosols traveled from the sea level to 1200 m; and (2) between December 22nd to 29th, 2014, when air masses migrated from the Indian Ocean (Fig. 1b) traveling for a long route of more than 3500 km over the Antarctic border and ice sheet, with fewer marine influence. In this case, sea salt aerosols have traveled in altitudes between 1000 and 3000 km. Analogous atmospheric transport was previously described in some studies^{32,33} and surveyed the change in marine ions concentrations from the Antarctic border to the inland, indicating a steady decrease as one moves away from the edge of the sea ice and also a relationship with the ice sheet altitude³⁴. Aerosol dynamics over the Southern Ocean/South Atlantic Sector are highly influenced by the westerly winds and cyclones that migrate typically around latitude 60°S or come from the western side of South America and move eastward. At the Weddell Sea, they may receive the influence of the clockwise Weddell low-pressure system that turns the air masses southeast to the Antarctic continent and influence the large-scale Weddell Gyre.

The application of STMX/NEXAFS and CCSEM/EDX techniques for particle analysis were complementary. They allow the characterization of field-collected particles' structure and chemical composition and infer their possible role in atmospheric reactions. For the individual particles analyzed by STMX/NEXAFS, we obtained the size distributions (Fig. 2a), which contain every single particle imaged/mapped representing the whole STXM/NEXAFS sample size. The particles were identified and classified by classes (See Methods) expressed in area equivalent diameter (μm), derived from the particle area, which is obtained by counting pixels exceeding a specific absorption level using a post vs. pre-absorption edge image of the particle. This allowed distinguishing aerosol classes as dust predominated below 0.5 μm (17 particles of 102), NaCl particles with nitrate (NO₃) (31 particles), particles containing ammonium sulfate

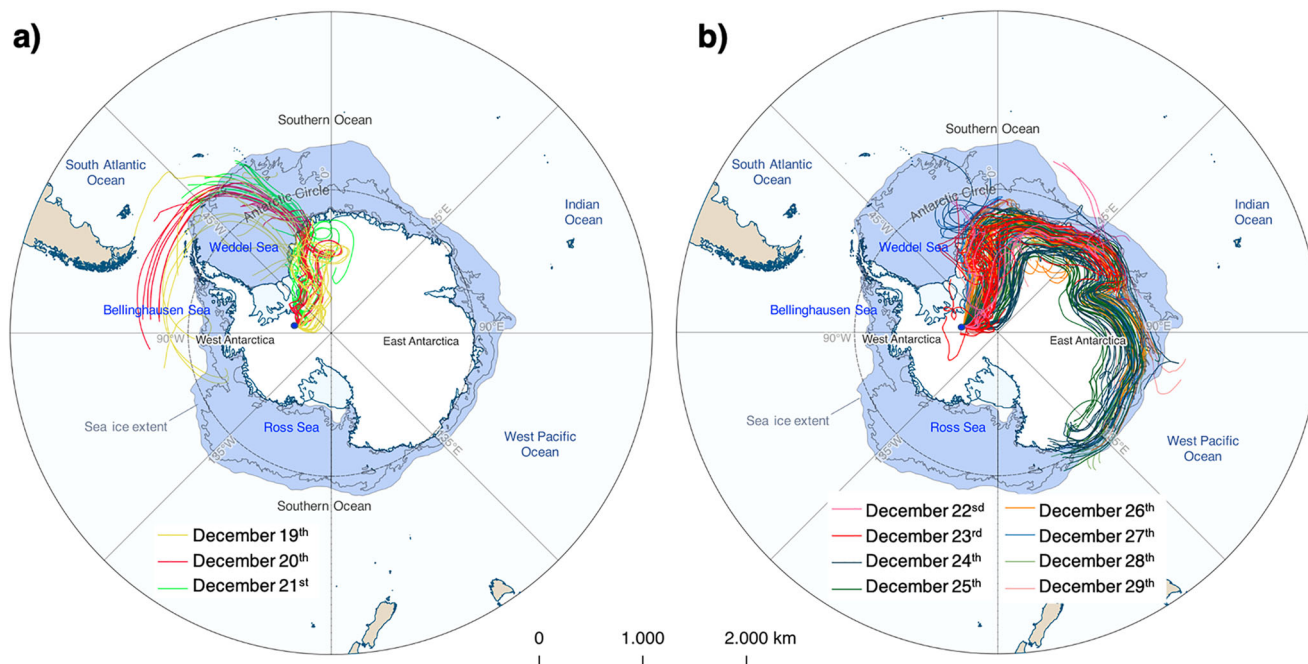


Fig. 1 Air masses backward trajectories. The backward trajectories using the Hybrid Single-Particle Lagrangian Integrated Trajectory (HYSPLOT/NOAA) model with Global Data Assimilation System (see “Methods”) were generated for the aerosol sampling periods of (a) December 19th to 21st, 2014; and (b) December 22nd to 29th, 2014. The backward trajectories were computed daily at 00:00 UTC at 10 m above ground level with 240-h durations each. The sea ice extent corresponds to the period of aerosol sampling, and the endpoint (blue dot) is the Criosfera 1 lab (84°,00’S; 79°,30’W). All maps were generated using QGIS free software and the Quantartica package from Norwegian Polar Institute (<https://www.npolar.no/quantartica/>).

$(\text{NH}_4)_2\text{SO}_4$ (8 particles), and three groups of particles enriched with chlorine oxides (Cl_xO_y). 46 of the 102 particles investigated contained a mixture of Cl_xO_y species (more details in Supplementary Table 1). A compiled panel from chemical STMX maps depicting individual particles with contributions of Cl_xO_y is presented in Fig. 2b. Henceforth, for clarity of indication, the nomenclature of Cl_xO_y will be used to represent the chlorine oxides and their intermediates.

It is possible to assume from the abundance of Cl and O in an unknown ratio of chlorine oxides were identified from: (1) the observation of high absorption levels at the Cl L-edge and O K-edge while missing absorption peaks at the C and N K-edges as well as S, Ca and K L-edges; (2) distinct differences in spectral features from NaCl-Spectra at the Cl L-edge, within the sample and against standard reference (see Supplementary Fig. 2). The use of STMX/NEXAFS herein was not able to distinguish the several possible forms of Cl_xO_y associated with the mixing state of aerosols (e.g., ClO_4^- , ClO_3^- , ClO_2^- or OCl^-), or the ion Cl^- , due to a lack of an acceptable reference to construct a standard spectrum of particle composition.

CCSEM/EDX analyzed a large particles ensemble showed that the sea salt particles (more than 2,000 particles of the total 3,300 analyzed) are substantially depleted of chlorine (Fig. 3) since Cl/(Na+0.5Mg) ratios (weight ratios) are well below 1 (marked by the dashed line)²⁴. If the formation of nitrate and sulfate had quantitatively balanced all missing chlorine, a ratio of $(\text{Cl} + \text{N} + 0.5 \text{S}) / (\text{Na} + 0.5 \text{Mg})$ calculated for individual particles would be near 1^{24,35}. However, most of the $(\text{Cl} + \text{N} + 0.5 \text{S}) / (\text{Na} + 0.5 \text{Mg})$ values of individual particles are about 0.5, indicating that the formation of sulfates and nitrates does not account for the observed chloride loss. Therefore, the formation of additional products contributes to chlorine depletion. More specifically, the role of the photochemical process on these sea salt particles for the subsequent formation of sodium nitrate (NaNO_3) can be found elsewhere²⁰.

Globally, estimations using the GEOS-Chem model indicated that atmospheric aging of sea salt particles contributes 85% to tropospheric inorganic chlorine³⁶. In Antarctica, a depletion of chloride relative to sodium is observed over most of the year, reaching a maximum of $\sim 20 \text{ ng m}^{-3}$ in spring when there are still large sea-salt amounts and acidic atmospheric components²¹. Here, the combined results of STMX/NEXAFS and CCSEM/EDX revealed that during the sea salt modifications by atmosphere multi-phase reactions, Cl becomes depleted in NaCl aged particles (see Ratios Fig. 3), while nitrates, sulfates, and NaClO_x are formed, as summarized in Fig. 4. Furthermore, the “missing chlorine” fraction in the sea salt particles over the snowpack corresponds to that fraction from the tropospheric chlorine budget, which is the chlorine oxides generated from snowpack byproduct reactions. The particle’s elemental microanalysis in Fig. 2a suggests that the unaccounted Cl depletion is likely a result of OH reactions that result in NaOH/ NaClO_x ($x = 2-4$) mixtures in dry particles, resulting in remaining detected particles as a mixture of chlorine oxides in their composition by heterogeneous interactions involving snowpack byproducts. Our findings are supported by previous reports showing that snowpack geochemistry and the rate of photolysis reactions have increased considerably since the onset of ozone depletion (between the 1970s and 1990s) at some Antarctic locations⁹.

Very intriguingly are the compositional maps of the existing distinct particles rich in O and Cl, occasionally alone, shown in purple in Fig. 2b. These particles are likely related to NaCl particles oxidized by OH radicals, which concentrations are higher from November to January in Antarctica³⁷. Ozone hole events expressively increased OH radical production in Antarctica³⁸, with a typically highly elevated level during the austral summer³⁹ and exhibited a mean level of OH around $3.9 \times 10^5 \text{ molecule cm}^{-3}$, as observed in Halley Research Station³⁷. In laboratory conditions, heterogeneous reactions of OH with deliquesced NaCl particles resulted in the formation of hydroxide (OH^-),

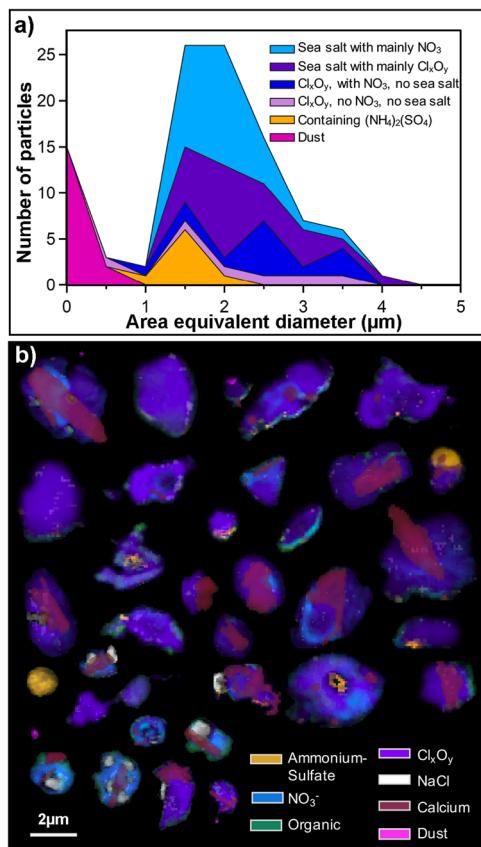


Fig. 2 Individual particles analyzed by STMX/NEAXFS. **a** The size distribution of classified particles based on the rule-based particle classification (see “Methods”); **b** composite image of individual particles (three-dimension visualization) that contain amounts of Cl_xO_y , compiled from chemical maps from different fields of view.

hypochlorite (OCl^-), and $\text{Cl}_{2(g)}$ products through ion-enhanced interfacial chemistry at the air-water interface^{40–42}. Previous studies and laboratory experiments of NaCl particles show that reaction with OH (gas-phase) generates OH^- and OCl^- species in the deliquesced sea salt particles that form $\text{NaCl}/\text{NaOH}/\text{NaClO}_x$ precipitates when they dehydrate^{41,43}. The rapidly hydrolyzed NaCl in a basic solution of molecular chlorine can occur, and some of $\text{Cl}_{2(g)}$ may be taken up in the particles to form OCl^- ⁴¹. In acid conditions, the HOCl (Cl precursor and reactive form to oxidation of chloride) would be released to the atmosphere as a gas phase, producing ClO^- ($K = 3.4 \times 10^{-8} \text{M}$)⁴⁴ in deliquesced particles and snow surfaces. As a consequence of the oxidation, the stabilization of NaOCl particles at a pH higher than 10.3 indicated an increase in particle alkalinity.

The long atmospheric pathway of sea salt particles from the Maritime Antarctic zone into the West Antarctic Ice Sheet (WAIS) (Fig. 1) allows enough space and time for effectively processing and modifying its aerosol structure. In Fig. 4, we present a conceptual model involving sea salt aerosol main reactions from the sea’s surface to the inland ice sheet. Changes in Cl/Na of sea salt may take place as a function of both biogeochemical and photolytic processes: (1) sea salt as aerosol particles can react with $\text{HNO}_{3(g)}$ and $\text{H}_2\text{SO}_{4(aq)}$, which is an oxidation byproduct of the dimethyl sulfide (DMS), a gas produced by the marine phytoplankton and bacterial cleavage of extracellular dimethyl sulfoniopropionate (DMSP)⁴⁵. In the Antarctic region, these sea salt interactions (hereafter the process called sulfatization) mainly occur in the Southern Ocean and near the sea ice edge, where marine biological activity is more intense⁴⁶. The key

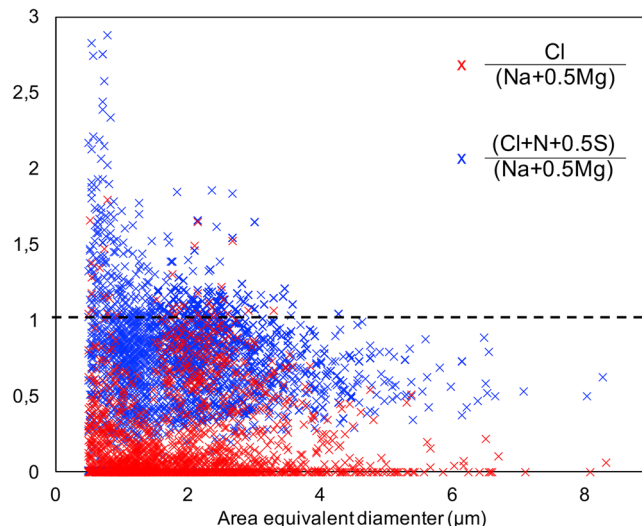


Fig. 3 Evaluation of sea salt aging process. The elemental composition of bulk particles was determined with CCSEM/EDX for all particles (2022) assigned as “sea salt” (See Supplementary Fig. 1); the ratios of $\text{Cl}/(\text{Na}+0.5\text{Mg})$ were calculated, where the dashed line indicates the characteristic ratio of unprocessed (i.e., fresh) sea salt particles. The values of $(\text{Cl}+\text{N}+0.5\text{S})/(\text{Na}+0.5\text{Mg})$ correspond to aged sea salt particles with chloride quantitatively displaced by only nitrate and sulfate.

factor in forming sulfuric and nitric acids is the OH radicals and hydrogen dioxide (HO_2) (originated from the photolysis of O_3 , hydrogen peroxide (H_2O_2), and nitrogen oxides (NO_x))³⁷. Both $\text{H}_2\text{SO}_{4(aq)}$ and $\text{HNO}_{3(g, aq)}$ induce partial dechlorination of sea-salt⁴⁷. The variability and intensification of the sulfatization also depend on dust concentration in the atmosphere since many sulfates and chloride salts may adhere to silicate minerals²⁵; (2) sea salt particles undergo fractionation during the long-range transport over the WAIS where chemical reactions with OH and NO_2 produced from in situ by a photolytic process of the snowpack, acting as the secondary mechanism to dechlorination of sea-salt particles. This results in forming particles containing chlorine oxides and $\text{Cl}_{(g)}$ radicals^{41,43,44,48}. Fig. 2b shows the coexistence of both biogeochemical and photolytic processes over sea salt.

Fig. 5 depicts a compilation of records, illustrating the impact of enhanced UV-B radiation over the polar stratosphere-troposphere. Depletion of stratospheric ozone has been enhanced since the 80’s decade (Fig. 5a), with a consequent increase in the mean actinic flux at 300 nm (Fig. 5b)⁴⁹, emphasizing the substantial radiative changes affecting the inner Antarctic areas. Meanwhile, ion perchlorate (ClO_4^-) recorded concentrations in the Geographic South Pole⁵⁰ (Fig. 5c) accompanied the progressive ozone loss when concentrations decreased to levels below approximately 240 DU (Fig. 5a). Ion perchlorate is present in the Antarctic environment and is part of the ionic composition of the snow, firm, and ice⁵¹. It is postulated a stratospheric origin for the perchlorate, assuming that chemical targets are present as gaseous chlorine, O_3 , and OH radicals^{28,29,52}. The ClO_4^- is one of the substances that contribute to the photochemical process of ozone loss in the Antarctic stratosphere (i.e., it could be generated when short wave UV-B radiation (<200 nm) interacted with chlorofluorocarbon molecules at the surface of polar stratospheric clouds (PSCs), which then reacted with ozone⁵²). In Antarctica, background (i.e., pre-ozone detected) ClO_4^- is in the order of 5 ng L^{-1} and has presented a systematic increase to more than 100 ng kg^{-1} since the mid-1970s in Geographic South Pole⁵⁰. A reanalysis of ionic ratios of Cl/Na^+ from two ice cores conducted at WAIS^{53,54} (Fig. 5d,e) dated from the mid-20th century depicted a detectable change when levels

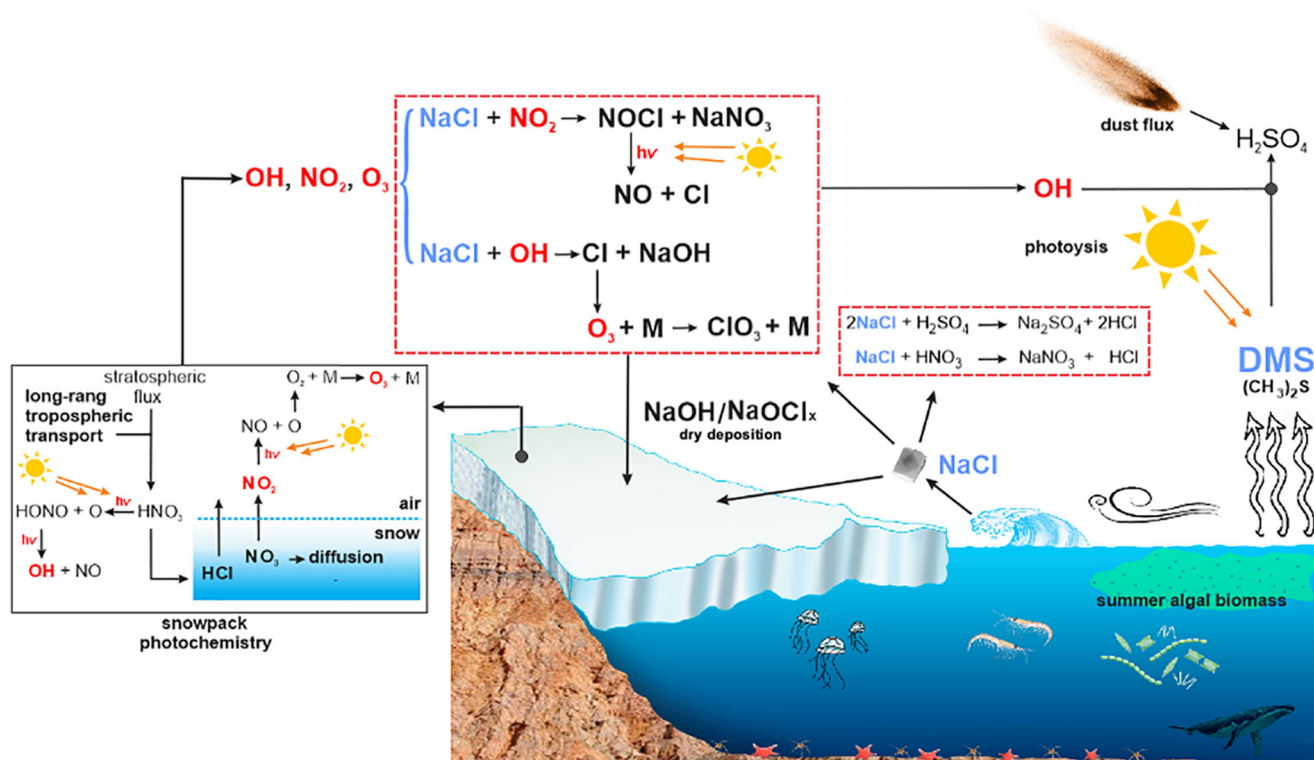


Fig. 4 Sea salt transformation in the troposphere. Schematic diagram illustrating possible chemical pathways to produce tropospheric chlorine-rich species in Antarctica.

of ozone reached 120 DU. Once volcanic eruptions are one pathway to injection of Cl to the stratosphere, the anomalous Cl/Na ratio observed during the ozone depletion period cannot be attributed to only volcanism^{55–57}. Based on the last survey of the Global Volcanism Program (<https://volcano.si.edu/>), from the mid-20th century to the present, the statistics of volcanic explosivity index (VEI), showed a relatively constant number of events with VEI > 4⁵⁸.

Fig 6 indicates monthly variations of measurements and parameters in Antarctica, evaluating the processes of sea salt. Fig 6a shows measured monthly Cl and Na at Dome Summit South⁵⁹, accompanying the Antarctic Sea ice extent (NOAA, <https://www.climate.gov/>) (Fig. 6b). One may observe that sea salt modification from sulfatization and heterogeneous reactions may peak in different seasons in Antarctica (summer and spring, respectively). Here, we used atmospheric concentration of aerosol between 2.5 and 10 nm in diameter (CN_{2.5–10})⁶⁰ measurements from the Bellingshausen Sea and the Weddell Sea as a proxy of the period of maximum sulfatization effect (Fig. 6c). Ozone depletion (Fig. 6d) occurs nearly the sea ice maximum extension phase (Fig. 6b) when sea salt aerosols are higher than in the summer season. Therefore, in that period, we may find a higher probability and, consequently, a higher contribution of the heterogeneous reactions to the indirect effect. Sulfatization peaks are in January–February (blue box) when there is a predominance of fresh biogenic aerosols near the Antarctic coast. The ozone column measurements in Fig. 6d are indicated by months. Considering our aerosol sampling period (December 19th to 29th, 2014), before the peak of the sulfatization period, the above considerations explain the strong contribution of heterogeneous reactions we found in our aerosol data.

Two other additional mechanisms may also contribute to the Cl/Na ratio anomaly but are related to Na: (1) aerosols emitted from fresh sea ice derived from frost flowers. These salty formations exhibit variable fractionation and are typically depleted in sulfate

and sodium relative to seawater ions due to the loss of mirabilite (Na₂SO₄) during the brine formation before frost flowers grow^{61,62}. Sodium depletion in frost flowers may reach around 10%, although other studies have reported more saline than sea water⁶³. Ionic ratios of Cl/Na measured from frost flowers in Halley Research Station presented the value of 2.04, while seawater samples ranged from 1.91 to 2.05 (SMOW value is 1.79)⁶². Therefore, emissions from frost flowers could not explain the considerable difference in Cl/Na before and during the ozone depletion period restricted to the spring to winter season, and; (2) Na from mineral dust. Although, in the last decades, mineral dust reaching Antarctica has increased^{64,65}. These processes may induce stronger westerly winds⁶⁶ and more northerly air mass advectations⁶⁷. Nevertheless, there is no evidence that this mechanism could have any implication for the Cl/Na, considering the modern dust levels in the atmosphere compared to the glacial periods.

To assess how intense the “excess chlorine” observed in modern times, we compared present ice core data with Holocene records (10k years B.P.). The comparison in Fig. 7 used Cl/Na data extracted from ice cores at different sites in the Antarctic continent (WAIS, Dome C, Geographic South Pole, Byrd Station, and Vostok)^{30,53,54,65,68,69}. Holocene data (before the ozone depletion period) is normally distributed and well-adjusted in the range of Antarctic aerosols²³. Prior work³⁰ indicated that Cl/Na values near the Antarctic coast are very close to bulk seawater (1.8) and increase at the edge of the Antarctic plateau. Cl/Na from our supporting databases, since 1980, depicts a log-normal distribution with systematic values above 4. From our investigated databases, before the ozone depletion period, only rare events surpassed VEI 4.0 and were attributed to volcanic events, and 95% were found between VEI 2.0 and 4.0. To the best of our knowledge, although most Holocene data do not have the same resolution as modern data, derived from upper ice core layers, ratios higher than 20, as found in the last decades, were

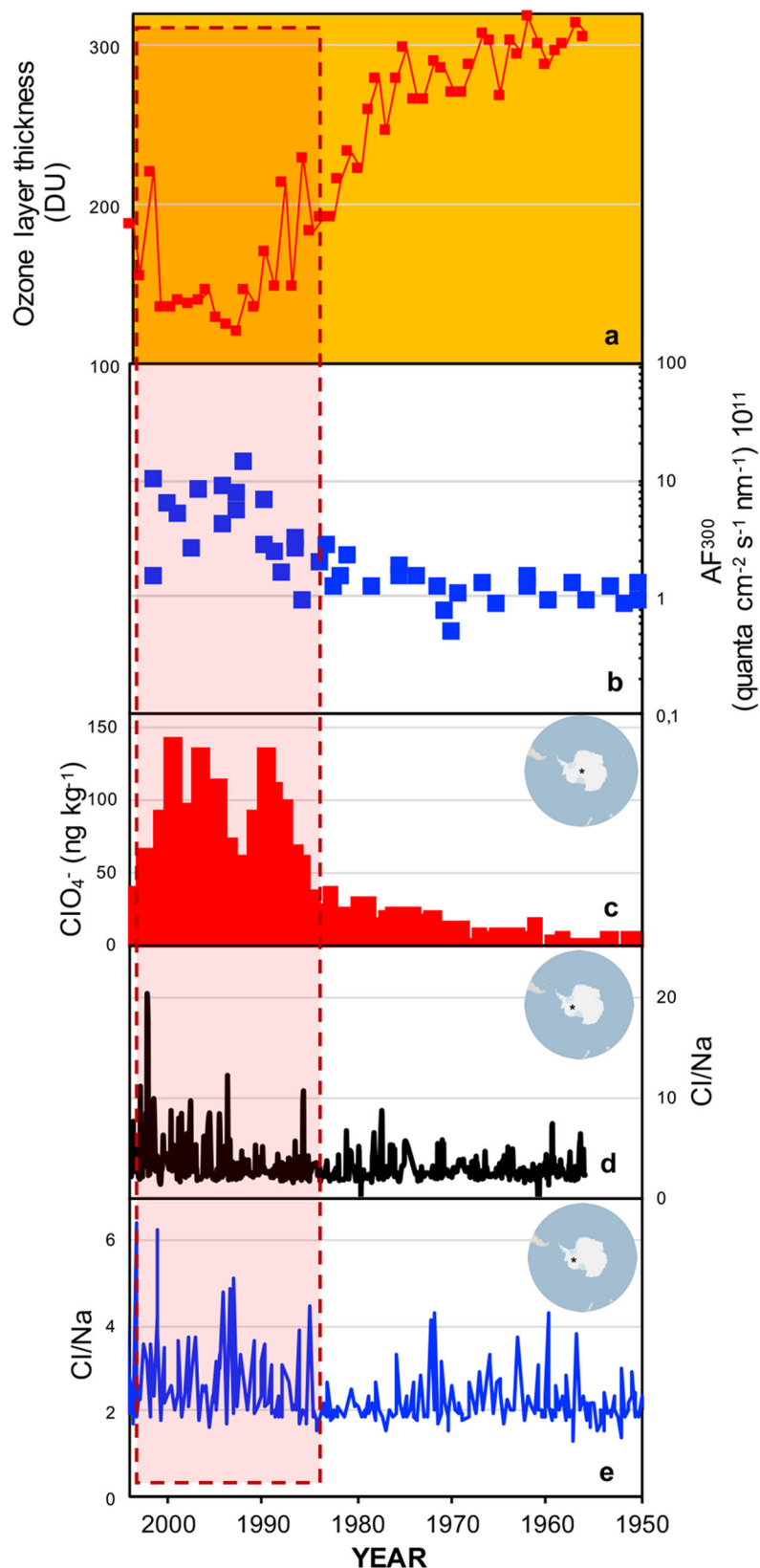


Fig. 5 The impact of the modern enhanced UV-B radiation on chlorine chemistry in Antarctic ice cores. **a** Temporal variability of October mean total ozone column over the Antarctic region in Dobson (DU) units; **(b)** the modeled radiative light that affects the Antarctic surface due to ozone hole formation by mean sunlit Actinic Flux at 300 nm⁴⁹ **(c)** Perchlorate concentrations in the Geographic South Pole ice core⁵⁰; **(d)** reanalysis from Cl/Na in a WAIS core⁵³; and **(e)** the temporal profile of the Cl/Na ratios for the period 1950–2004 at Mount Johns⁵⁴.

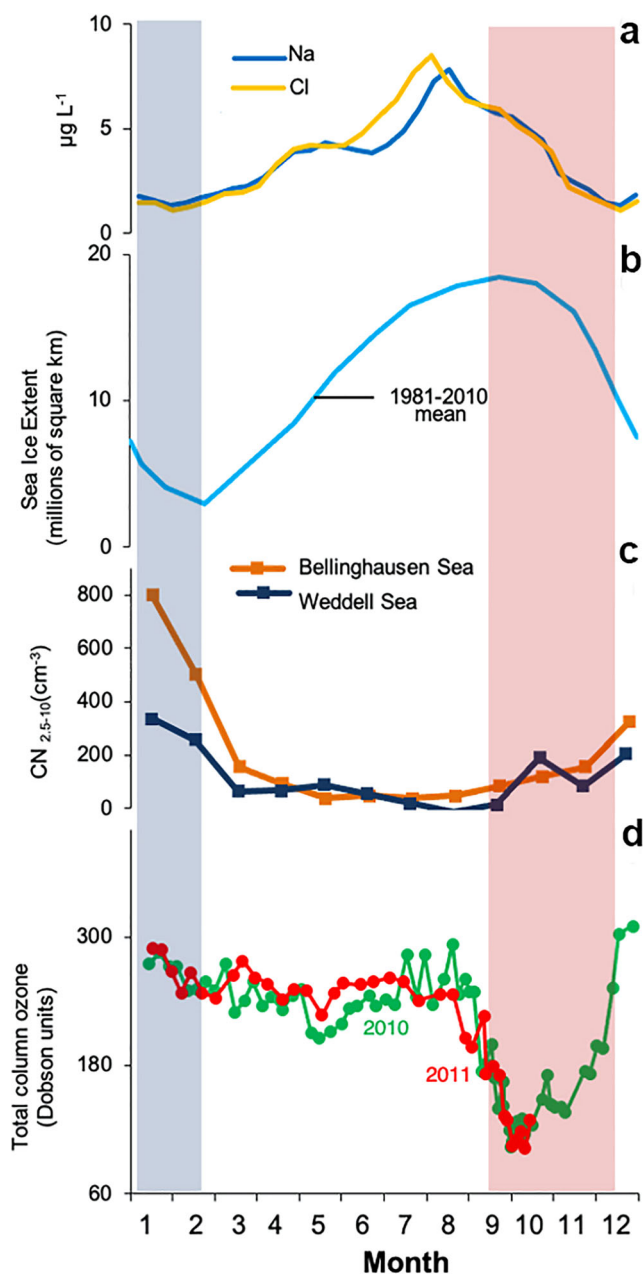


Fig. 6 Seasonal behavior in sea salt processing in Antarctica interconnection with geochemistry parameters. Monthly data of (a) Antarctica (Dome Summit South) seasonal variations for mean concentrations of Cl and Na⁵⁹; (b) Antarctic sea ice extent; (c) the concentration of aerosol particles (CN) between 2.5 and 10 nm in diameter in the Maritime Antarctica⁶⁰; and (d) monthly ozone column. Boxes are indicating periods when sulfatization (blue box) and heterogeneous reactions (red box) reach maximum contributions.

unprecedented (Fig. 5d). Our reanalyzed data show that aerosol chlorine geochemistry is by far more impacted by incoming UV-B radiation than by concurrent impacts such as volcanic eruptions and dechlorination from mineral dust interactions.

Sea-salt aerosols directly affect the total Earth's radiation balance by scattering the incoming solar radiation, absorbing the outgoing terrestrial radiation, and indirectly acting as cloud condensation nuclei (CCN), contributing to cloud formation⁷⁰. It is estimated that sea salt aerosols exert a noteworthy direct radiative effect in the Southern Ocean with seasonal means

ranging from -2 to -3 W m^{-2} . In contrast, its indirect radiative forcing exceeds this range, reaching a seasonal mean of -4 W m^{-2} ⁷¹. For comparison, the modern concentrations of CO_2 contribute around $+1.85 \text{ W m}^{-2}$ to climate forcing⁷². Additionally, modified sea salt aerosols can also act as CCN because of their hygroscopicity.

The ozone depletion in Antarctica created a unique scenario to investigate photochemical processes in both the polar stratosphere and troposphere. Most projections agree that the ozone layer will recover to the pre-1970 level around 2100⁷³. Two important outcomes derived from our measurements and data processing: (1) intense interactions of sea salt particles with snowpack geochemical byproducts pointedly increased chlorine depletion from sea salt. This is confirmed by individual particles mapping from combined techniques of STMX/NEXAFS and CCSEM/EDX at the molecular scale and by Cl/Na ratios in WAIS ice cores at the “geochemical scale” and, (2) even though during the last 10k years Cl/Na ratios exhibited punctual higher values than the bulk seawater signature due to several factors as volcanism and probably to post-depositional processes, in the recent time period, modern Cl/Na ratios values reached frequently remarkable levels.

Finally, our results point to the need to deeply investigate the sea salt chemical interactions from the sea surface emissions to deposition in ice sheets (marine and cryosphere compartments), which is crucial to model the net radiation balance in Antarctica satisfactorily.

Materials and methods

Aerosol sampling. Airborne particles were collected in the remote laboratory Criosfera 1 lab ($84^\circ,00'S$; $79^\circ,30'W$) at 1,280 meters above the sea level, which belongs to the Brazilian Antarctic Program (<http://criosfera1.com>). It is located between the Geographic South Pole and the Ellsworth Mountains and has been powered only by solar and wind energy since 2012. At that site, air temperatures range from -3 to $-55 \text{ }^\circ\text{C}$ (<https://legacy.bas.ac.uk/met/READER/>). Samplings were conducted continuously from December 19th to 29th, 2014, under ultra-clean conditions, away from any in situ human emissions. During sampling, the mean air temperature was $-14.1 \text{ }^\circ\text{C}$ with no snowfall; the average wind speed was 3.6 m s^{-1} , with a maximum of 12 m s^{-1} . After collection, the samples were placed in sealed hermetic boxes that preserved the sample in a closed ambient (preventing external contamination), transported to Brazil, and stored in a desiccator (20-30% relative humidity) pending laboratory analysis.

For the integrated aerosols sampling, we used a May cascade impactor⁷⁴ with aerodynamic diameters ranging from 0.5 to $4.0 \text{ }\mu\text{m}$ maintained at a constant airflow rate of 17.5 L min^{-1} . The air inlet was fixed 4 meters above the snow surface. Samples were collected on Si_3N_4 films supported by silicon wafers (Silson, Inc.) and TEM grids (Carbon type B film, Copper 400 mesh grids; Ted Pella, Inc.).

CCSEM/EDX. The CCSEM/EDX (Computer Controlled Scanning Microscopy coupled with Energy Dispersive X-ray) microanalysis was conducted over 3,300 particles at the Environmental Molecular Science Laboratory (Pacific Northwest National Laboratory, Richland, USA) using an FEI Quanta field emission gun environmental SEM X-ray spectrum was acquired at an accelerating voltage of 20 kV with a beam current of 500 pA. The elements used for identifying particle types were C, N, O, Na, Mg, Al, Si, P, S, Cl, K, Ca, Mn, Fe, and Zn. More details of the technique and analysis are published in related works^{24,75}.

The total bulk particles (3,300) were classified manually into five groups (sea salt, sea salt mixed with sulfate, carbonaceous, sulfates, and dust) based on their elemental composition. More information on bulk particles classification is available in Supplementary Notes.

STMX/NEXAFS. We have employed synchrotron-based multi-element Scanning Transmission X-ray Microscopy with near-edge X-ray absorption fine structure spectroscopy (STXM/NEXAFS)³¹ at the Advanced Light Source at Lawrence Berkeley National Laboratory. The measurements were performed at beamlines 5.3.2.2 (carbon, oxygen, and nitrogen data) and 11.0.2.2 (chlorine and sulfur data) with mapping techniques using spectral features at S, Cl, and Ca L-edges and C, N, and O K-edges. The mapping of compounds was obtained using soft X-rays from 160 eV (Sulfur L-edge) to 546 eV (Oxygen K-edge). Data analysis is performed using MATLAB[®]-code in a semi-automatic way. The script for N, S, O, and Cl was written based on the standard spectra and the carbon script described in previous studies^{76,77}.

A total of 102 individual particles from the Criosfera 1 lab site were analyzed to obtain spatially resolved information on chemical heterogeneity and spatially resolved chemical bonding information for these elements on individual

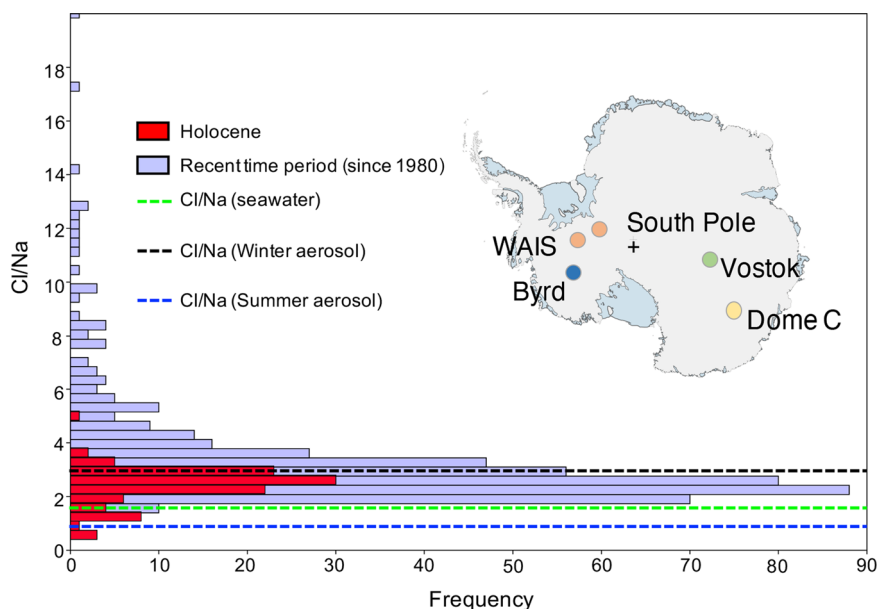


Fig. 7 Cl/Na ratios for the recent period and from Holocene. Comparison of modern and Holocenic Cl/Na in ice cores and aerosols over a recent period from WAIS ice cores^{53,54}; last 10k years B.P. period in Dome C^{30,65}, Vostok Station³⁰, Byrd Station^{30,68} and in the Geographic South Pole⁶⁹. The dotted lines indicate an average Cl/Na (1.8) of bulk seawater³⁰; average of Cl/Na in aerosol (fine mode) measurements in summer (1.4) (blue) and winter (3.3)²³.

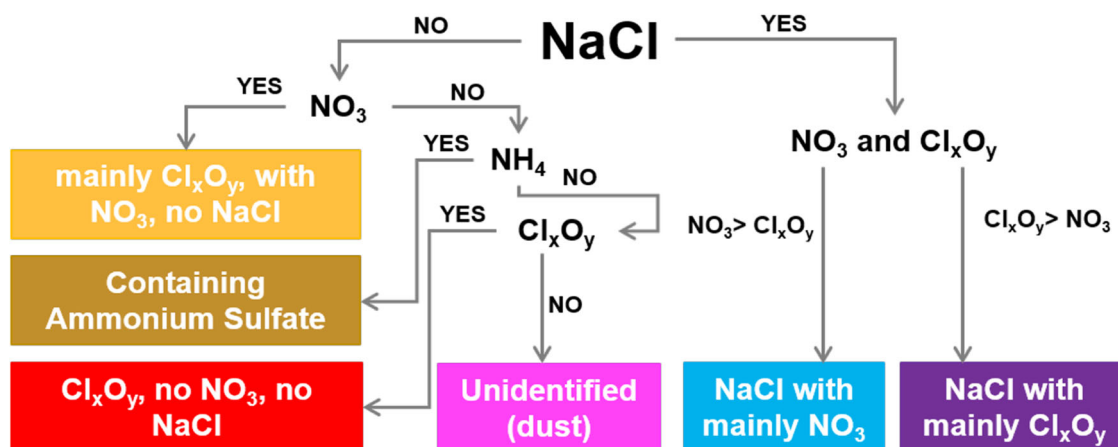


Fig. 8 Individuals' rule-based cluster classification. The rule-based cluster classification for individuals was applied to separate and classify 102 particles into clusters.

particles^{24,78–80}. A rule-based classification (Fig. 8) was applied to separate the particles into clusters, resulting in six major classes and their mixing states: NaCl with mainly NO_3 , NaCl with mainly Cl_xO_y , mainly Cl_xO_y with NO_3 and no NaCl, Ammonium Sulfate ($(\text{NH}_4)_2\text{SO}_4$), Cl_xO_y with no NO_3 and no NaCl, and dust. Additional experimental details of STXM spectra and standards used to analyze the samples are included in Supplementary Information. The instrument and its operation are described in detail by Kilcoyne et al. (2003)³¹.

HYSPLIT trajectory model. The Hybrid Single-Particle Lagrangian Integrated Trajectory (HYSPLIT) model uses a hybrid concept of Lagrangian and Eulerian approaches. Once the Lagrangian model uses a moving frame of reference for the advection and diffusion calculations as the trajectories or air parcels move from their initial location, the Eulerian uses a fixed three-dimensional grid to compute air concentrations⁸¹. The trajectory model simulates air parcel movement by wind advection using spatially and temporally gridded meteorology and geomorphological data, and it is widely used to establish potential source locations of atmospheric pollutant transport and dispersion in both forward and backward modes.

The HYSPLIT/NOAA model is a computer free available that allows the computing of air parcel trajectories of atmospheric components⁸² and can be run interactively through the ARL READY system (<https://www.ready.noaa.gov/index.php>). Here, the model was calculated the backward trajectories using the Global Data Assimilation System at 10 m above ground level and running daily (sampling period December 19th to 29th, 2014) with endpoints at the Criosfera 1 lab ($84^\circ 00'$

$W79^\circ 30'$). The backward trajectories were computed daily at 00:00 UTC with 240-hour duration each.

Supporting databases. To support our study, we used a database of ionic measurements of ice cores from diverse points in Antarctica in two different ages: (a) for the recent time period, were reanalyzed two ice cores from the WAIS at Mount Johns ($79^\circ 55' 28'' \text{ S}$, $94^\circ 23' 18'' \text{ W}$)⁵⁴, and in a shallow core (IC-3/Ufrgs, $85^\circ 59' \text{ S}$, $81^\circ 35' \text{ W}$)⁵³ retrieved during a Chilean–Brazilian Antarctic traverse in the summer of 2004/2005; additionally, we compared the ionic ratios with ClO_4^- (perchlorate) data from an ice core of the Geographic South Pole⁵⁰; (b) from Holocene period through Geographic South Pole ice-cores record⁶⁹; at Dome C^{30,65}; in Vostok Station³⁰; and at Byrd Station^{30,68}. Also, we used an aerosol measurement monitored continuously in Maritime Antarctica/northern Antarctic Peninsula ($62^\circ 05' \text{ S}$, $058^\circ 24' \text{ W}$) between 1985 and 1993 in week resolution²³.

Reporting summary. Further information on research design is available in the Nature Portfolio Reporting Summary linked to this article.

Data availability

The CCSEM/EDX and STMX/NEXAFS raw data used in Figs. 2 and 3 and Supplementary material are available at <https://doi.org/10.5281/zenodo.7674968>⁸³. All NEXAFS regions

maps and images used in Fig. 2b are available at <https://doi.org/10.5281/zenodo.7674995>⁸⁴. The HYSPLIT/NOAA model and air parcel trajectories in Fig. 1 are open-access and can be obtained from <https://www.ready.noaa.gov/index.php>⁸². The database of ionic measurements of ice cores and aerosols is presented in Figs. 5c and d, 6c and 7 were retrieved from varied sampling points in Antarctica^{23,30,50,53,54,59,65,68,69}. The ozone time series data plotted in Figs. 5a and 6d are available at National Oceanic and Atmospheric Administration - NOAA (<https://www.esrl.noaa.gov/gmd/grad/neubrew/SatO3DataTimeSeries.jsp>). The Antarctic Sea ice extent in Fig. 6b was based on Charctic data from the National Snow and Ice Data Center (<https://nsidc.org/arcticseaicenews/charctic-interactive-sea-ice-graph/>), and the data are available at NOAA (www.climate.gov).

Code availability

The STMX/NEXAFS standard spectra and script for particle individual analysis of N, S, O, and Cl, that were performed using MATLAB® code in a semi-automatic way, were based on Moffet et al. (2010)⁶⁹ (<https://www.mathworks.com/matlabcentral/fileexchange/29085-stxm-spectromicroscopy-particle-analysis-routines>), which was further developed by Piens et al. (2016)⁷⁰.

Received: 21 July 2022; Accepted: 28 February 2023;

Published online: 16 March 2023

References

- Solomon, S. et al. Emergence of healing in the Antarctic ozone layer. *Science* **353**, 269–274 (2016).
- Turner, J. et al. Non-annular atmospheric circulation change induced by stratospheric ozone depletion and its role in the recent increase of Antarctic sea ice extent. *Geophys. Res. Lett.* **36**, L08502 (2009).
- Bornman, J. F. et al. Solar ultraviolet radiation and ozone depletion-driven climate change: effects on terrestrial ecosystems. *Photochem. Photobiol. Sci.* **14**, 88–107 (2015).
- Iii, D. J. E., Sulzberger, B., G. Zepp, R. & Austin, T.A. Effects of stratospheric ozone depletion, solar UV radiation, and climate change on biogeochemical cycling: interactions and feedbacks. *Photochem. Photobiol. Sci.* **14**, 127–148 (2015).
- Rozema, J., Boelen, P. & Blokker, P. Depletion of stratospheric ozone over the Antarctic and Arctic: Responses of plants of polar terrestrial ecosystems to enhanced UV-B, an overview. *Environ. Pollut.* **137**, 428–442 (2005).
- Singh, J., Dubey, A. K. & Singh, R. P. Antarctic terrestrial ecosystem and role of pigments in enhanced UV-B radiations. *Rev. Environ. Sci. Biotechnol.* **10**, 63–77 (2011).
- Bernhard, G. H., McKenzie, R. L., Lantz, K. & Stierle, S. Updated analysis of data from Palmer Station, Antarctica (64° S), and San Diego, California (32° N), confirms large effect of the Antarctic ozone hole on UV radiation. *Photochem. Photobiol. Sci.* **21**, 373–384 (2022).
- Cordero, R. R. et al. Persistent extreme ultraviolet irradiance in Antarctica despite the ozone recovery onset. *Sci. Rep.* **12**, 1266 (2022).
- Jones, A. E. & Wolff, E. W. An analysis of the oxidation potential of the South Pole boundary layer and the influence of stratospheric ozone depletion. *J. Geophys. Res. Atmos.* **108**, 1–7 (2003).
- Li, J., Ma, X., von Salzen, K. & Dobbie, S. Parameterization of sea-salt optical properties and physics of the associated radiative forcing. *Atmos. Chem. Phys.* **8**, 4787–4798 (2008).
- Murphy, D. M. et al. Influence of sea-salt on aerosol radiative properties in the Southern Ocean marine boundary layer. *Nature* **392**, 62–65 (1998).
- Wilson, T. W. et al. A marine biogenic source of atmospheric ice-nucleating particles. *Nature* **525**, 234–238 (2015).
- Hara, K. et al. Important contributions of sea-salt aerosols to atmospheric bromine cycle in the Antarctic coasts. *Sci. Rep.* **8**, 13852 (2018).
- Tian-Kunze, X. et al. Sea ice as a source of sea salt aerosol: A trajectory study of 25 years of year-round sea salt aerosol record at Neumayer, Antarctica. *EPIC3 Geophys. Res. Abstracts* **11**, 8934–2 (2009).
- Frey, M. M. et al. First direct observation of sea salt aerosol production from blowing snow above sea ice. *Atmos. Chem. Phys.* **20**, 2549–2578 (2020).
- Boredy, S. K. R. & Kawamura, K. A 12-year observation of water-soluble ions in TSP aerosols collected at a remote marine location in the western North Pacific: an outflow region of Asian dust. *Atmos. Chem. Phys.* **15**, 6437–6453 (2015).
- Finlayson-Pitts, B. J. Reactions at surfaces in the atmosphere: integration of experiments and theory as necessary (but not necessarily sufficient) for predicting the physical chemistry of aerosols. *Phys. Chem. Chem. Phys.* **11**, 7760–7779 (2009).
- Xiao, H.-W., Xiao, H.-Y., Shen, C.-Y., Zhang, Z.-Y. & Long, A.-M. Chemical composition and sources of marine aerosol over the Western North Pacific Ocean in Winter. *Atmosphere* **9**, 298 (2018).
- Bigler, M., Röthlisberger, R., Lambert, F., Stocker, T. F. & Wagenbach, D. Aerosol deposited in East Antarctica over the last glacial cycle: Detailed apportionment of continental and sea-salt contributions. *J. Geophys. Res. Atmos.* **111**, 1–14 (2006).
- Gonçalves, S. J. Jr. et al. Photochemical reactions on aerosols at West Antarctica: A molecular case-study of nitrate formation among sea salt aerosols. *Sci. Total Environ.* **758**, 143586 (2021).
- Legrand, M. et al. Year-round records of bulk and size-segregated aerosol composition in central Antarctica (Concordia site) – Part I: Fractionation of sea-salt particles. *Atmos. Chem. Phys.* **17**, 14039–14054 (2017).
- Hara, K. et al. Horizontal distributions of aerosol constituents and their mixing states in Antarctica during the JASE traverse. *Atmos. Chem. Phys.* **14**, 10211–10230 (2014).
- Correia, A. L. Aerossóis Atmosféricos na Antártica: Sazonalidade, Composição Elementar e Relação com “El Niño”. (1998).
- Laskin, A. et al. Tropospheric chemistry of internally mixed sea salt and organic particles: Surprising reactivity of NaCl with weak organic acids. *J. Geophys. Res. Atmos.* **117**, 1–12 (2012).
- Iizuka, Y. et al. Sulphate and chloride aerosols during Holocene and last glacial periods preserved in the Talos Dome Ice Core, a peripheral region of Antarctica. *Tellus B: Chem. Phys. Meteorol.* **65**, 20197 (2013).
- Jones, A. E., Weller, R., Wolff, E. W. & Jacobi, H.-W. Speciation and rate of photochemical NO and NO₂ production in Antarctic snow. *Geophys. Res. Lett.* **27**, 345–348 (2000).
- Oum, K. W., Lakin, M. J., DeHaan, D. O., Brauers, T. & Finlayson-Pitts, B. J. Formation of molecular chlorine from the photolysis of ozone and aqueous sea-salt particles. *Science* **279**, 74–76 (1998).
- Dasgupta, P. K. et al. The origin of naturally occurring perchlorate: the role of atmospheric processes. *Environ. Sci. Technol.* **39**, 1569–1575 (2005).
- Kang, N., Anderson, T. A. & Jackson, W. A. Photochemical formation of perchlorate from aqueous oxychlorine anions. *Anal. Chimica Acta* **567**, 48–56 (2006).
- Legrand, M. R. & Delmas, R. J. Formation of HCl in the Antarctic atmosphere. *J. Geophys. Res.* **93**, 7153–7168 (1988).
- Kilcoyne, A. L. D. et al. Interferometer-controlled scanning transmission X-ray microscopes at the Advanced Light Source. *J. Synchrotron Radiation* **10**, 125–136 (2003).
- Gassó, S. & Stein, A. F. Does dust from Patagonia reach the sub-Antarctic Atlantic Ocean? *Geophys. Res. Lett.* **34**, 1–5 (2007).
- Li, F., Ginoux, P. & Ramaswamy, V. Transport of Patagonian dust to Antarctica. *J. Geophys. Res. Atmos.* **115**, 1–9 (2010).
- Li, C. et al. Spatial and temporal variability of marine-origin matter along a transect from Zhongshan Station to Dome A, Eastern Antarctica. *J. Environ. Sci.* **46**, 190–202 (2016).
- Laskin, A., Iedema, M. J. & Cowin, J. P. Quantitative time-resolved monitoring of nitrate formation in sea salt particles using a CCSEM/EDX single particle analysis. *Environ. Sci. Technol.* **36**, 4948–4955 (2002).
- Wang, X. et al. Global tropospheric halogen (Cl, Br, I) chemistry and its impact on oxidants. *Atmos. Chem. Phys.* **21**, 13973–13996 (2021).
- Bloss, W. J. et al. Observations of OH and HO₂ radicals in coastal Antarctica. *Atmos. Chem. Phys.* **7**, 4171–4185 (2007).
- Qian, J., Mopper, K. & Kieber, D. Photochemical production of the hydroxyl radical in Antarctic waters. *Deep Sea Res. Part I: Oceanogr. Res. Pap.* **48**, 741–759 (2001).
- Mauldin, R. et al. South Pole Antarctica observations and modeling results: New insights on HOx radical and sulfur chemistry. *Atmos. Environ.* **44**, 572–581 (2010).
- Knipping, E. M. et al. Experiments and simulations of ion-enhanced interfacial chemistry on aqueous NaCl aerosols. *Science* **288**, 301–306 (2000).
- Laskin, A. et al. Reactions at interfaces as a source of sulfate formation in sea-salt particles. *Science* **301**, 340–344 (2003).
- Oum, K. W., Lakin, M. J., DeHaan, D. O., Brauers, T. & Finlayson-Pitts, B. J. Formation of molecular chlorine from the photolysis of ozone and aqueous sea-salt particles. *Science* **279**, 74–76 (1998).
- Finlayson-Pitts, B. J. The tropospheric chemistry of sea salt: A molecular-level view of the chemistry of NaCl and NaBr. *Chem. Rev.* **103**, 4801–4822 (2003).
- Davis, D. et al. South Pole NOx chemistry: an assessment of factors controlling variability and absolute levels. *Atmos. Environ.* **38**, 5375–5388 (2004).
- Kiene, R. P., Linn, L. J. & Bruton, J. A. New and important roles for DMSP in marine microbial communities. *J. Sea Res.* **43**, 209–224 (2000).
- Iizuka, Y. et al. The rates of sea salt sulfatization in the atmosphere and surface snow of inland Antarctica: SEA SALT SULFATIZATION IN ANTARCTICA. *J. Geophys. Res.* **117**, 1–11 (2012).
- Brink, H. Mten Reactive uptake of HNO₃ and H₂SO₄ in sea-salt (NaCl) particles. *J. Aerosol Sci.* **29**, 57–64 (1998).

48. Vogt, R. & Finlayson-Pitts, B. J. A diffuse reflectance infrared Fourier transform spectroscopic study of the surface reaction of NaCl with gaseous NO₂ and HNO₃. *J. Phys. Chem.* **98**, 3747–3755 (1994).
49. Spolaor, A. et al. Antarctic ozone hole modifies iodine geochemistry on the Antarctic Plateau. *Nat. Commun.* **12**, 5836 (2021).
50. Jiang, S., Cox, T. S., Cole-Dai, J., Peterson, K. M. & Shi, G. Trends of perchlorate in Antarctic snow: Implications for atmospheric production and preservation in snow. *Geophysical Research Letters* **43**, 9913–9919 (2016).
51. Jackson, A. et al. Deposition, accumulation, and alteration of Cl⁻, NO₃⁻, ClO₄⁻ and ClO₃⁻ salts in a hyper-arid polar environment: Mass balance and isotopic constraints. *Geochimica et Cosmochimica Acta* **182**, 197–215 (2016).
52. Rao, B., Anderson, T. A., Redder, A. & Jackson, W. A. Perchlorate formation by ozone oxidation of aqueous chlorine/oxy-chlorine species: Role of Cl x O y radicals. *Environ. Sci. Technol.* **44**, 2961–2967 (2010).
53. De Mello Marques, M. et al. Analysis of an Antarctic ice core by ion chromatography (Mg²⁺, Na⁺, Cl⁻, and SO₄²⁻ content). *Geochimica Brasiliensis* **28**, 89–96 (2014).
54. Thoen, I. U., Simões, J. C., Lindau, F. G. L. & Sneed, S. B. Ionic content in an ice core from the West Antarctic Ice Sheet: 1882–2008 A.D. *Braz. J. Geol.* **48**, 853–865 (2018).
55. Coffey, M. T. Observations of the impact of volcanic activity on stratospheric chemistry. *J. Geophys. Res.* **101**, 6767–6780 (1996).
56. Thamban, M. et al. Aerosol perturbations related to volcanic eruptions during the past few centuries as recorded in an ice core from the Central Dronning Maud Land, Antarctica. *Curr. Sci.* **91**, 1200–1207 (2006).
57. Tabazadeh, A. & Turco, R. P. Stratospheric chlorine injection by volcanic eruptions: HCL Scavenging and implications for ozone. *Science* **260**, 1082–1086 (1993).
58. Global Volcanism Program. Volcanoes of the World. Venzke, E. (ed.). *Smithsonian Institution* **4**, 10–4, (2013).
59. Curran, M. A. J., Ommen, T. D. V. & Morgan, V. Seasonal characteristics of the major ions in the high-accumulation Dome Summit South ice core, Law Dome, Antarctica. *Ann. Glaciol.* **27**, 385–390 (1998).
60. Jang, E. et al. New particle formation events observed at the King Sejong Station, Antarctic Peninsula – Part 2: Link with the oceanic biological activities. *Atmos. Chem. Phys.* **19**, 7595–7608 (2019).
61. Rankin, A. M., Wolff, E. W. & Martin, S. Frost flowers: Implications for tropospheric chemistry and ice core interpretation. *J. Geophys. Res.: Atmos.* **107**, AAC 4-1–AAC 4-15 (2002).
62. Rankin, A. M., Auld, V. & Wolff, E. W. Frost flowers as a source of fractionated sea salt aerosol in the polar regions. *Geophys. Res. Lett.* **27**, 3469–3472 (2000).
63. Martin, S., Drucker, R. & Fort, M. A laboratory study of frost flower growth on the surface of young sea ice. *J. Geophys. Res.: Oceans* **100**, 7027–7036 (1995).
64. McConnell, J. R., Aristarain, A. J., Banta, J. R., Edwards, P. R. & Simões, J. C. 20th-Century doubling in dust archived in an Antarctic Peninsula ice core parallels climate change and desertification in South America. *PNAS* **104**, 5743–5748 (2007).
65. Röthlisberger, R. et al. Limited dechlorination of sea-salt aerosols during the last glacial period: Evidence from the European Project for Ice Coring in Antarctica (EPICA) Dome C ice core. *J. Geophys. Res. Atmos.* **108**, 1–6 (2003).
66. Cataldo, M. et al. Mineral dust variability in central West Antarctica associated with ozone depletion. *Atmos. Chem. Phys.* **13**, 2165–2175 (2013).
67. Dixon, D. A. et al. An ice-core proxy for northerly air mass incursions into West Antarctica. *Int. J. Climatol.* **32**, 1455–1465 (2012).
68. Palais, J. M. & Legrand, M. Soluble impurities in the Byrd Station ice core, Antarctica: Their origin and sources. *J. Geophys. Res.* **90**, 1143 (1985).
69. Winski, D. A. et al. Seasonally resolved Holocene sea ice variability inferred from South Pole ice core chemistry. *Geophys. Res. Lett.* **48**, e2020GL091602 (2021).
70. Wise, M. E. et al. Depositional ice nucleation onto crystalline hydrated NaCl particles: a new mechanism for ice formation in the troposphere. *Atmos. Chem. Phys.* **12**, 1121–1134 (2012).
71. Ayash, T., Gong, S. & Jia, C. Q. Direct and indirect shortwave radiative effects of sea salt aerosols. *J. Clim.* **21**, 3207–3220 (2008).
72. Oshima, N. et al. Global and Arctic effective radiative forcing of anthropogenic gases and aerosols in MRI-ESM2.0. *Progr. Earth Planet. Sci.* **7**, 38 (2020).
73. Dhomse, S. S. et al. Delay in recovery of the Antarctic ozone hole from unexpected CFC-11 emissions. *Nat. Commun.* **10**, 1–12 (2019).
74. May, K. R. An “ultimate” cascade impactor for aerosol assessment. *J. Aerosol Sci.* **6**, 413–419 (1975).
75. Laskin, A., Cowin, J. P. & Iedema, M. J. Analysis of individual environmental particles using modern methods of electron microscopy and X-ray microanalysis. *J. Electr. Spectrosc. Relat. Phenomena* **150**, 260–274 (2006).
76. Moffet, R. C., Henn, T., Laskin, A. & Gilles, M. K. Automated chemical analysis of internally mixed aerosol particles using X-ray spectromicroscopy at the carbon K-edge. *Anal. Chem.* **82**, 7906–7914 (2010).
77. Piens, D. S. et al. Measuring mass-based hygroscopicity of atmospheric particles through in situ imaging. *Environ. Sci. Technol.* **50**, 5172–5180 (2016).
78. Moffet, R. C. et al. Spectro-microscopic measurements of carbonaceous aerosol aging in Central California. *Atmos. Chem. Phys.* **13**, 10445–10459 (2013).
79. Moffet, R. C., Tivanski, A. V. & Gilles, M. K. Scanning transmission X-ray microscopy: applications in atmospheric aerosol research. <https://www.osti.gov/biblio/1005004> (2011).
80. Laskin, A., Gilles, M. K., Knopf, D. A., Wang, B. & China, S. Progress in the analysis of complex atmospheric particles. *Annu. Rev. Anal. Chem. (Palo Alto Calif)* **9**, 117–143 (2016).
81. Stein, A. F. et al. NOAA’s HYSPLIT atmospheric transport and dispersion modeling system. *Bull. Am. Meteorol. Soc.* **96**, 2059–2077 (2015).
82. Draxler, R. R. & Rolph, G. D. HYSPLIT (HYbrid Single-Particle Lagrangian Integrated Trajectory) model access via NOAA ARL READY website (<http://ready.arl.noaa.gov/HYSPLIT.php>), NOAA Air Resources Laboratory. *Silver Spring, MD* **25**, 1 (2010).
83. Gonçalves Jr., S. J. et al. Raw data set used for a paper by Gonçalves Jr. et al. [Data set]. <https://doi.org/10.5281/zenodo.7674968> (2023).
84. Gonçalves Jr., S. J. et al. NEXAFS images and raw data set used for a paper by Gonçalves Jr. et al. <https://doi.org/10.5281/zenodo.7674995> (2023).

Acknowledgements

Part of this work was Financed by CAPES – Brazilian Federal Agency for Support and Evaluation of Graduate Education within the Ministry of Education of Brazil, process 99999.002847/2015-09 and 99999.001833/2015-04. CNPq-MCTI/INCT-Criosfera 573720/2008 for logistics support. S. M. (INPE) for fundamental engineering support. LARAMG (UERJ) for background support. CCSEM/EDX was performed at Environmental Molecular Sciences Laboratory, a national scientific user facility sponsored by OBER at PNNL. PNNL is operated by the U.S. Department of Energy by Battelle Memorial Institute under contract DE-AC06-76RL0. STXM/NEXAFS analysis at beamline 11.0.2.2 of the Advanced Light Source at Lawrence Berkeley National Laboratory is supported by the Director, Office of Science, Office of Basic Energy Sciences of the U.S. Department of Energy under Contract No. DE-AC02-05CH11231. Beamline 11.0.2.2 also acknowledges support from the Office of Basic Energy Sciences Division of Chemical Sciences, Geosciences, and Biosciences by the Condensed Phase and Interfacial Molecular Sciences Program of the U.S. Department of Energy. M. K. G., T. H., J. W., and S. M. (Lawrence Berkeley National Laboratory group) acknowledge support from the U.S. Department of Energy’s Atmospheric System Research program, an Office of Science, Office of Biological and Environmental Research (OBER). J. W., S. M., and T. H. acknowledge the student exchange program between the University of Würzburg and U.C. Berkeley (curator Professor A. Forchel, Würzburg and NSF IGERT program at UCB, DGE-0333455, Nanoscale Science and Engineering - From Building Blocks to Functional Systems). The authors gratefully acknowledge the NOAA Air Resources Laboratory (ARL) for the provision of the HYSPLIT transport and dispersion model and READY website (<http://www.ready.noaa.gov>) used in this publication. We acknowledge the Norwegian Polar Institute’s Quantarctica package.

Author contributions

S.J.G.Jr., H.E., R.H.M.G. conducted the project, leading the conceptualization, methodology, sampling, formal analysis, investigation, writing of original draft, final review & final editing; J.W., T.H., S.C., S.M. performed the laboratory experiments; M.G., A.L., C.I.Y. provided technical support and helped with results interpretation; M.M.M., J.C.S. provided the ice cores database and helped with discussions; H.R.P., M.S. supported the sampling; N.d.M.N., B.V.X.d.O. contributed to data analysis and interpretation. All authors contributed to manuscript preparation and writing. All authors contributed equally to manuscript preparation and agreed to the final version of the manuscript.

Competing interests

The author declares no competing interests.

Additional information

Supplementary information The online version contains supplementary material available at <https://doi.org/10.1038/s43247-023-00739-z>.

Correspondence and requests for materials should be addressed to Sérgio J. Gonçalves Jr.

Peer review information : *Communications Earth & Environment* thanks Keiichiro Hara and the other, anonymous, reviewer(s) for their contribution to the peer review of this work. Primary Handling Editors: Tuija Jokinen and Clare Davis. Peer reviewer reports are available.

Reprints and permission information is available at <http://www.nature.com/reprints>

Publisher’s note Springer Nature remains neutral with regard to jurisdictional claims in published maps and institutional affiliations.



Open Access This article is licensed under a Creative Commons Attribution 4.0 International License, which permits use, sharing, adaptation, distribution and reproduction in any medium or format, as long as you give appropriate credit to the original author(s) and the source, provide a link to the Creative Commons license, and indicate if changes were made. The images or other third party material in this article are included in the article's Creative Commons license, unless indicated otherwise in a credit line to the material. If material is not included in the article's Creative Commons license and your intended use is not permitted by statutory regulation or exceeds the permitted use, you will need to obtain permission directly from the copyright holder. To view a copy of this license, visit <http://creativecommons.org/licenses/by/4.0/>.

© The Author(s) 2023